Confined Water in Tunnel Nanopores of Sepiolite: Insights from Molecular Simulations

Jinhong Zhou[1], Xiancai Lu[1*], Edo S Boek[2]

1 State Key Laboratory for Mineral Deposits Research, School of Earth Sciences and Engineering, Nanjing University, Nanjing 210023, China

2 Department of Chemical Engineering, Imperial College London, London SW7 2AZ, United Kingdom

Running title: *Confined Water in Tunnels of Sepiolite*

* Corresponding author.

Email: xcljun@nju.edu.cn

Tel: +86 25 89681065

Fax: +86 25 89680703

Highlights

- **GCMC-based calculated water adsorption isotherm of sepiolite indicates that the tunnel pores are fully filled with zeolitic water with RH>5%.**
- **New four-site model of zeolitic water is proposed according to molecular dynamics simulation.**
- **Strong confining effects on the zeolitic water of intrapore surface of sepiolite are revealed clearly.**

Abstract

Sepiolite is a type of magnesium-rich fibrous clay mineral. The unique fibrous structure endows it with various applications in many fields. Revealing the behavior of confined water in sepiolite nanopores is crucial to understand the macroscopic properties of sepiolite. Aiming to ascertain the distribution and dynamics of confined water, molecular simulations using grand canonical Monte Carlo and molecular dynamics methods have been performed. We obtain the water adsorption isotherm, density distribution profiles and dynamic information of confined waters in sepiolite tunnels. We find that zeolitic water is very hard to be desorbed from sepiolite under ambient conditions. Based on the distribution profile and trajectories of the water, we reveal the accurate distribution sites and propose a new distribution model of the confined water including one bound water site and four zeolitic water sites which are determined by sepiolite lattice. The zeolitic water at different sites can exchange freely and frequently, and thus these sites may be energetically similar. This model provides more fundamental understanding of hydration of sepiolite, and highlights the water behaviors in the tunnel pores of microporous minerals, which are thought being controlled by the crystallographic structure. The much lower mobility of zeolitic water in sepiolite than that in montmorillonite implies that materials with nano-sized tunnel pores could have more efficient fixation on foreign molecules or ions in environmental applications than those layered materials with slit pores.

46 **Keywords:** Sepiolite, Zeolitic water, Adsorption isotherm, Molecular dynamics, Grand
47 canonical Monte Carlo

1. Introduction

Sepiolite is a typical fibrous Mg clay mineral, containing a 2:1 layer structure like other phyllosilicates. However, sepiolite only has continuous planes of basal oxygen atoms and lacks continuous octahedral sites which differs from other layer silicates and leads to tunnels. This structure could be described as ribbons of 2:1 phyllosilicate structures and each ribbon is connected with the next one by inversed SiO_4 tetrahedra (Galan, 1996). Due to its unique structure, sepiolite is comprehensively applied in many fields, such as special absorbent, cigarette filter, carrier of agricultural chemicals and catalysts, and so on (Anderson et al., 1993; Celis et al., 2000; Dogan et al., 2007; Giustetto et al., 2011a; Giustetto et al., 2011b; Gupta and Suhas, 2009; Kara et al., 2003; Ozcan and Ozcan, 2005; Samper-Madrigal et al., 2015; Sanchez et al., 2011; Shimizu et al., 2004). Sepiolite is proved to have the ability to adsorb heavy metal ions (e.g., Cu^{2+}, Zn^{2+}, Co^{2+})(Brigatti et al., 1996; Celis et al., 2000; Kara et al., 2003; Sheikhhosseini et al., 2014; Shimizu et al., 2004; Vico, 2003) and organic matter (Darder et al., 2007; Dogan et al., 2007; Hubbard et al., 2003; Ruiz-Hitzky, 2001; Rytwo et al., 2002; Shariatmadari et al., 1999). Delgado et al. successfully used sepiolite to remove CO_2 from CO_2/CH_4 gas mixture (Delgado et al., 2007).

The ideal formula of sepiolite is $Mg_8Si_{12}O_{30}(OH)_4(OH_2)_4{\cdot}nH_2O$, which rarely have heterovalent cation substitutions and layer charge. OH is the hydroxyl of octahedral sheet, and OH_2 is the bound water coordinated with octahedral magnesium at the edge of the tunnel. H_2O is zeolitic water in the tunnel. The amount of zeolitic water could change

with environmental relative humidity (RH), and therefore *n* is variable. The structure of sepiolite is hard to be determined by single-crystal diffraction methods due to its fine-grained and poor crystallinity. A widely accepted structure of sepiolite is a three zeolitic water sites model deduced by Brauner and Preisinger from X-ray diffraction experiments (Brauner and Preisinger, 1956).

With the applications of sepiolite increasing, more microscopic information at the atomic scale is needed. Especially a better characterization of the water confined in sepiolite is important to understand the behavior of the other foreign ions and molecules adsorbed into the tunnel. Therefore, the behavior of water on sepiolite is not only important to mineralogists, but also to the applications (Shimizu et al., 2004). The hydration and dehydration of sepiolite have been studied experimentally for decades (Bukas et al., 2013; Caturla et al., 1999; Frost and Ding, 2003; He et al., 1996; Rautureau and Mifsud, 1977; Tsampodimou et al., 2015). However, the details of intracrystalline water in sepiolite are still under debate, especially the water distribution sites in the tunnel pores. Brauner and Preisinger deduced three zeolitic water sites with topology (Brauner and Preisinger, 1956; Preisinger, 1959). Post et al. (2007) introduced the synchrotron-based powder X-ray diffraction method to investigate the dehydration of sepiolite, and they proposed a model of four zeolitic water sites which is different from previous topology results, and a folding structure with water loss (Post et al., 2007).

Compared with experiments, computational simulation methods could obtain more precise microscopic information than direct measurements and observation (Benli et al.,

2012; Ockwig et al., 2009). Ockwig et al. studied the hydrogen bonding patterns in sepiolite and palygorskite using computational simulations and experimental methods (Ockwig et al., 2009). And Benli et al. revealed the anisotropic characteristics of sepiolite using molecular dynamics simulations and experimental methods (Benli et al., 2012). In order to disclose more microscopic information of the confined water, we combine grand canonical Monte Carlo (GCMC) and molecular dynamics (MD) simulation methods to investigate the distribution and dynamics of the confined water in the tunnel nanopores of sepiolite. We simulate the water adsorption isotherm in intracrystalline pores of sepiolite with changing RH by using the GCMC method. The structures and dynamics of the confined water in tunnels with MD simulations have been acquired. Based on these results, we propose a new model of zeolitic water, and reveal the confining effect of sepiolite on the mobility of water in tunnels.

2. Models and Methods

2.1 Sepiolite models

The ideal formula of the constructed sepiolite is $Mg_8Si_{12}O_{30}(OH)_4{\cdot}4(OH_2){\cdot}nH_2O$. The cell parameters of sepiolite are: $a \times b \times c$ =13.405 × 27.016 × 5.275 Å^3, $\alpha = \beta = \gamma = 90°$, which are from Post et al. (Post et al., 2007). The box size of our model is $2 \times 2 \times 5$ unit cells (Fig. 1). The tunnel extends along the z axis. The simulation box is set as a 3D periodic box.

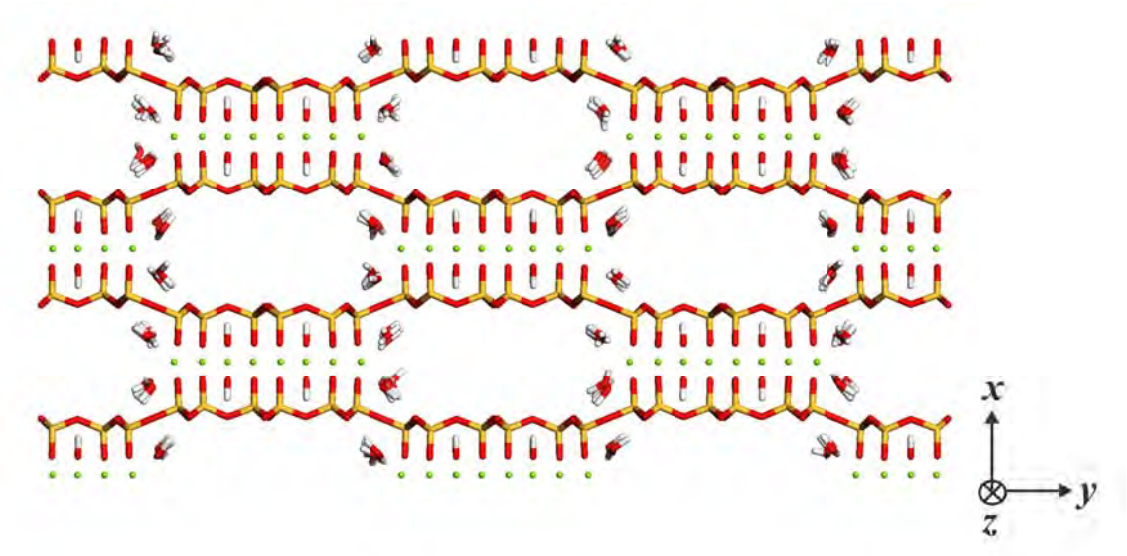

FIGURE 1. The initial model of sepiolite without zeolitic water molecule.

2.2 Method details

Monte Carlo (GCMC and MD simulation methods are employed to study the water adsorption isotherm, spatial distribution and diffusion of water under ambient conditions (1 atm, 298 K). The force field for clay and water is *CLAYFF* (Cygan et al., 2004), which has been verified by Ockwig et al. (Ockwig et al., 2009). GCMC simulations are carried out using the TOWHEE package (Martin, 2013), and MD simulations using the LAMMPS package (Plimpton et al., 2007).

At first, we run GCMC simulations in the constant (μVT) ensemble under different relative humidities. The chemical potential μ of water determines whether water molecules should be inserted in or removed from the sepiolite. The adsorption process is always in the environment with air and water vapor mixture. In the air and vapor mixture of water, the relative humidity (RH) could be described as (Tambach et al., 2004):

$$RH = \frac{81.7}{\phi(P_{water})} e^{-(\mu_w^{sat} - \mu_w)/RT} \quad (1)$$

where (P_{water}) is the fugacity coefficient at the given partial pressure of water. μ_w^{sat} and μ_w are the chemical potentials of water vapor at saturated and partial pressures, respectively. In Equation (1), the chemical potential of water is connected with RH. Therefore, different RH can be achieved by changing μ_w. In our study, we remove all zeolitic water in the initial models of sepiolite. We change the chemical potential of water to perform GCMC simulations and obtain the adsorption isotherm of zeolitic water. Every GCMC simulation runs for 15,000,000 steps to ensure adsorption equilibrium.

In order to disclose the dynamics of water in the tunnels, MD simulations are performed following the GCMC simulations. The final structure from the GCMC simulation under highest RH (water-saturated tunnels) is used as the initial structure in the following MD simulation. The MD simulation is run for 2 ns with a time step of 1 fs, and the last 1 ns is recorded for analysis. The electrostatic interactions are treated using the Ewald summation.

3. Results and Discussion

3.1 Water adsorption isotherm

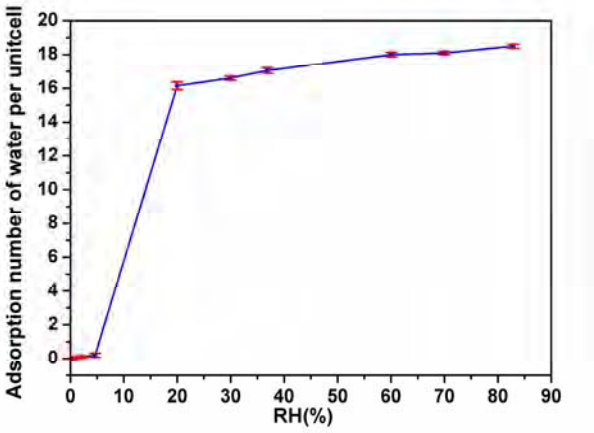

FIGURE 2. Water adsorption isotherm of sepiolite at 298 K derived from GCMC simulations.

From the GCMC simulations with changing relative humidity (RH), we derive the water adsorption isotherm for intracrystalline tunnels (Fig. 2). The water content here is merely for zeolitic water. Therefore this adsorption isotherm is incomparable with previous experiments, in which both intracrystalline and intercrystalline water adsorptions are included (Caturla et al., 1999). As the RH is always higher than 25% under experimental ambient conditions, it is generally hard to measure the water adsorption amount at RH < 25%. However, our simulations obtain the number of zeolitic water molecules from 0% RH and higher.

From the adsorption isotherm, we find that the number of zeolitic water stays at 0 within RH < 5%, which means that only bound water exists in the tunnel. While RH > 5%, the content of zeolitic water will jump up rapidly and zeolitic water fills the tunnels quickly. Therefore, zeolitic water always exists under ambient conditions. In contrast, it is difficult

for bound water to escape from the tunnels (Post et al., 2007).

3.2 Distribution model of confined water

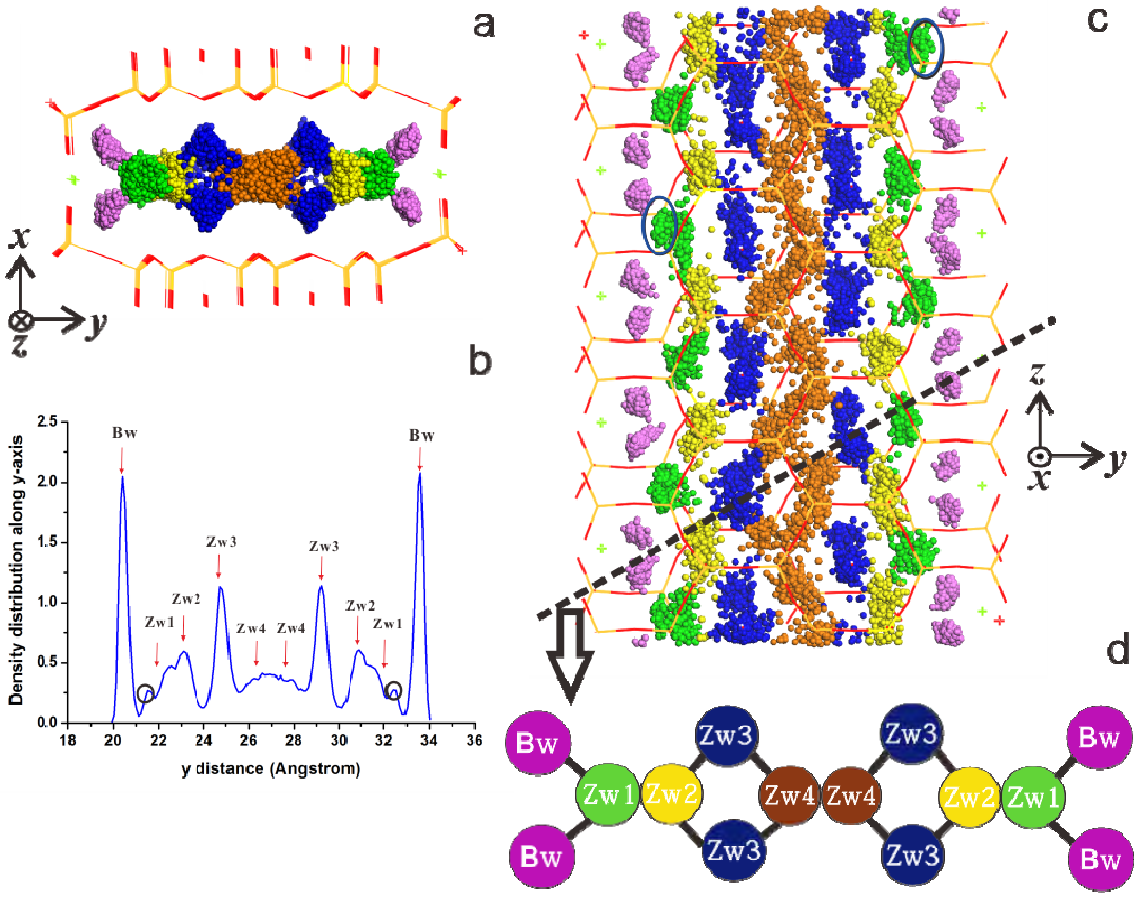

FIGURE 3. Distribution model of the confined water in sepiolite tunnel.

(a) Water trajectories in one tunnel, viewed by *xy*-cross section. (b) Density distribution profile along *y* axis of water in one tunnel. (c) Water trajectories in one tunnel, viewed by *yz*-cross section. (d) Distribution model for water in one tunnel, projected in cross section cut by the black dashed line in part c. Bw (purple) denotes the bound water site and Zw represents the zeolitic water site. Zw1 (green), Zw2 (yellow), Zw3 (dark blue) and Zw4 (light brown) denote different zeolitic sites. Black circles in (b) denote the water

molecules marked with blue ovals in (c).

In the sepiolite tunnel, there is only one type of bound water site. Bw sites correspond to the two sharp peaks (y= 20.5Å and 33.5Å) in both ends of the density distribution profile (Fig. 3b). The distribution of zeolitic water is still under debate. 3 zeolitic sites were deduced by Brauner and Preisinger (Brauner and Preisinger, 1956; Preisinger, 1959), and one additional zeolitic site was found by Post et al (Post et al., 2007). We propose a new 4 zeolitic water sites model (Fig. 3d) via the y-axis density distribution profile and the trajectories of water. However, the position of the additional site is different from that found by Post et al (Post et al., 2007).

The Zw1 site is the closest zeolitic water site to the bound water site (Bw), and also next to the Zw2 site closely. Zw1 sites is closely adjacent to the Zw2 ones along the y axis so that their density distribution profiles are overlapped and presents as broad peaks around 21~24 Å and 30~33 Å (Fig. 3b) although both sites can be identified in Fig. 3c. Some water molecules diffusing between Zw1 and Zw2 can be observed, which also leads to overlapped profiles. Part of the water molecules on Zw1 are attracted by the bound water, which is consistent to the small peaks around 21.5 Å and 32.5 Å on the density distribution profile (Fig. 3b). However, Zw2 site is not on the same xy-cross section with Zw1, and much closer to the Zw3 site (Fig. 3c).In the tunnel inner surface, there are two kinds of six-membered rings: one is linking the inversional tetrahedral sheets, and we mark this as edge six-membered ring; the other one is on the tetrahedral sheets, we mark

it as tetrahedral six-membered ring. The Zw3 site is adjacent to the Zw2 site and close to the center of tetrahedral six-membered rings, which is caused by the attraction of the hydroxyl groups located in the center of tetrahedral six-membered rings. Therefore the Zw3 sites have upper and lower positions constrained by the ceiling and bottom tetrahedral six-membered rings respectively. In addition, they are staggered as tetrahedral layers on the two sides. The distribution of Zw3 may explain that the surface of sepiolite is less hydrophobic than talc, which is proposed by Benli et al. (Benli et al., 2012). Connecting to the Zw3 sites, there are two equal positions of zeolitic water (Zw4) in tunnel center (Fig. 3d), which results in a board peak similar in distribution profile with Zw1 and Zw2 (Fig. 3b). Each Zw4 site links to the neighbor Zw3 sites (Fig. 3d). These two positions are equal crystallographically. Viewing from the *yz* cross section cut by the dashed line shown in Fig. 3c, these 4 zeolitic water sites could be projected in one planar graph and show a symmetrical distribution (Fig. 3d). Noticeably, this distributions is not precisely realistic in any plane.

Our four-site model is different from the distribution models proposed previously (Brauner and Preisinger, 1956; Post et al., 2007). Three-site model deduced by Brauner and Preisinger was the first model and has been accepted widely (Brauner and Preisinger, 1956). With the experimental methods developing, Post et al. recognized one additional zeolitic water site and proposed a new model (Post et al., 2007). In their models, three sites are similar to the Zw1, Zw3 and Zw4 sites in our model. The additional site of Post's model is different from that in our model (Zw2 site). The additional site in Post's model

occupies two positions (upper and lower) (Post et al., 2007). However, the additional site in our model (Zw2 site) only occupies one position in the middle as Zw1.

3.3 Bound water on edge Mg atoms

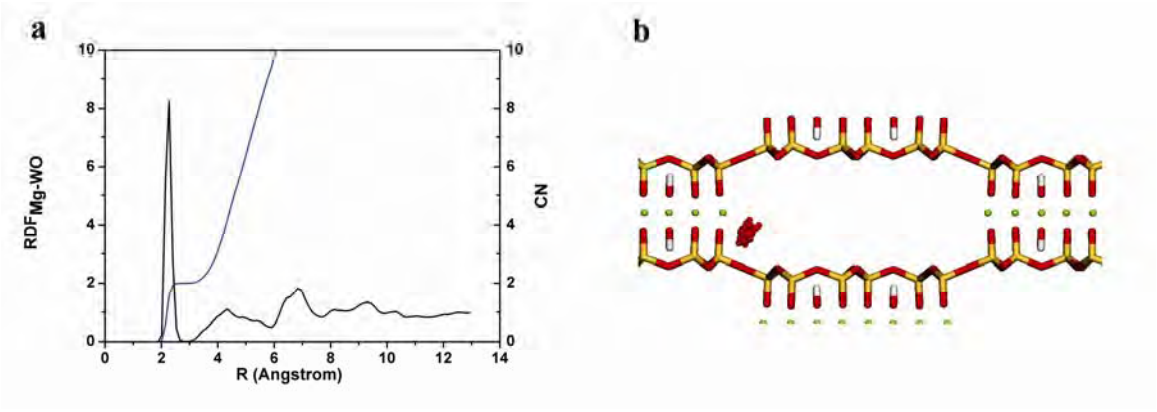

FIGURE 4. (a) Radial distribution function of water oxygen (WO) around edge Mg atoms; (b) 1 ns trajectory of one bound water molecule. For clarity, the other water molecules are removed.

Each edge Mg atom is strongly coordinated with two water molecules, which are bound waters corresponding to the sharp peak in the RDF curve of water around the edge Mg atoms (Fig. 4a). This result is consistent with the previous studies (Benli et al., 2012; Bukas et al., 2013; Caturla et al., 1999). This strong interaction could be also investigated by recording the trajectory of bound water molecules. Therefore we follow one bound water molecule and obtain its trajectory (Fig. 4b). It is clear that the bound water molecule only vibrates around the equilibrium position of the edge Mg and never leaves in the simulation. Therefore, it is considered that the bound water cannot be exchanged in the tunnel.

3.4 Zeolitic water

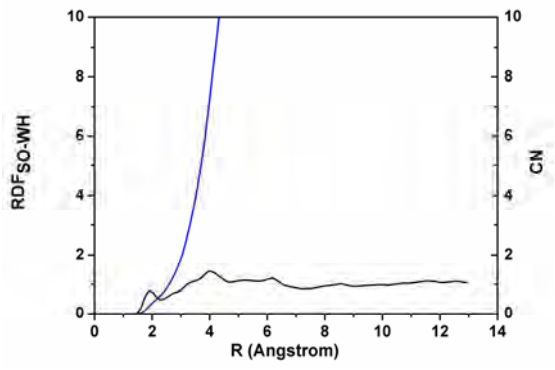

FIGURE 5. Radial distribution functions of water hydrogen (WH) around surface oxygen (SO) of sepiolite tunnel.

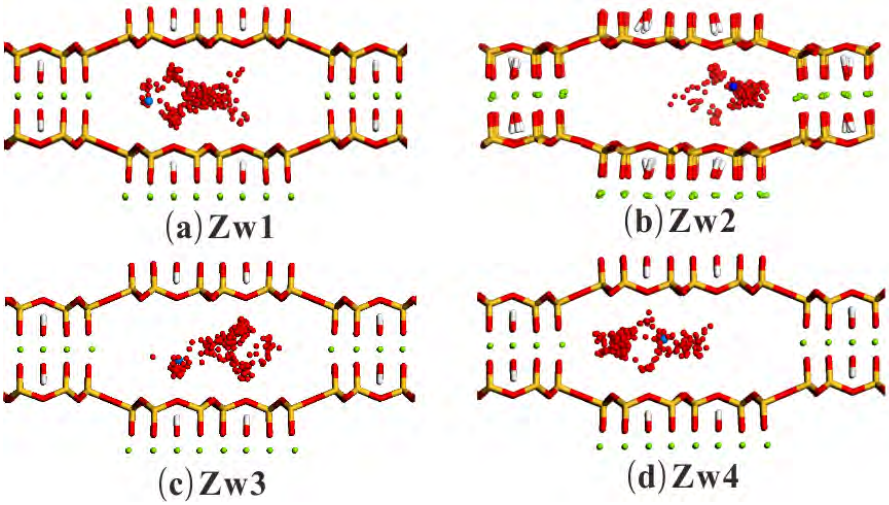

FIGURE 6. 1 ns trajectories of one zeolitic water molecule in each Zw site: (a) Zw1; (b) Zw2; (c) Zw3; (d) Zw4. Blue ball is the start position of the marked water molecule. For clarity, the other water molecules are removed.

The first peak located at 2.0 angstrom represents the interaction between the hydrogen atoms of bound water and the surface oxygen atoms (Fig. 5). However, zeolitic water does not show obvious interactions with the pore surface due to the relatively long

distance (~4.0 angstrom). We follow one zeolitic water molecule in every zeolitic site and obtain its trajectory to observe the motion of zeolitic water in different sites (Fig. 6). It is clear that zeolitic water at every site can diffuse to the other sites freely. Therefore, the zeolitic water molecules are not restrained by the sepiolite framework and can diffuse among all zeolitic sites. Thus, these zeolitic waters on four sites are thermodynamically indistinguishable.

3.5 Mobility of confined water

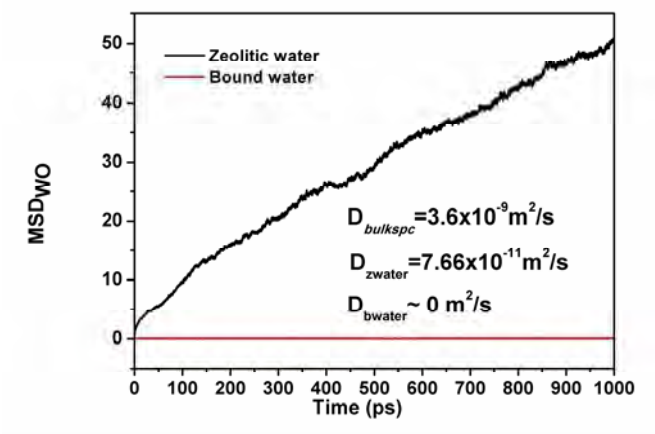

FIGURE 7. Mean squared displacement (MSD) curves of water in sepiolite. D is diffusion coefficient. $D_{blukspc}$ is from Zheng et al. (Zheng et al., 2012).

Diffusion coefficient is calculated from the slope of MSD curve. The diffusion coefficient of zeolitic water (D_{zwater}=7.66×10^{-11}m^2/s) (Fig. 7) is obviously higher than bound water (D_{bwater}≈0 m^2/s), as expected. Therefore the mobility of zeolitic water is larger than the bound water, which does not show obvious mobility due to the strong interaction with the edge magnesium atoms. These results are consistent with the trajectory results presented

254 above. Bound water only vibrates around the equilibrium position without any diffusion.
255 In contrast, zeolitic water in every site could diffuse freely in the tunnel. However, the
256 mobility of zeolitic water is two orders of magnitude lower than that of bulk SPC water.
257 According to previous researches, the diffusion coefficients of water in montmorillonite
258 (monolayer, bilayer and triple-layer hydrates) are all on the order around 10^{-9}~10^{-10} m^2/s,
259 which are lower than that of bulk SPC water (Holmboe and Bourg, 2013; Zhang et al.,
260 2014). That is to say, the confining effect of the unique sepiolite structure is more
261 significant than montmorillonite.

262 # 4. Implications

263 This study provides a physical basis for investigating the states and behaviors of the
264 waters in intra-particle and inter-particle pores of sepiolite. The calculated adsorption
265 isotherm of water shows that the tunnels of sepiolite are generally filled with zeolitic
266 water under ambient conditions and most of zeolitic water could be lost only under
267 extremely low RH (< 5%). In experimental studies on the dehydration of sepiolite, it is
268 hard to remove all zeolitic water and even bound water only by changing RH. High
269 temperature (maybe over 500 K) seems necessary for removing bound water in
270 experiments (Bukas et al., 2013; Post et al., 2007).
271 The proposed four-site model of zeolitic water in sepiolite provides a fundamental
272 understanding for sepiolite researches. It can be deduced that the other foreign molecules
273 in sepiolite may also show similar distribution sites as water molecules. This model of
274 sepiolite can be also taken as an analogue for the mineralogical researches and

implications of micro-porous minerals. For montmorillonites, layered crystal structures cause that interlayer water molecules show layering behaviors, such as monolayer, bilayer and trilayer (Anderson et al., 2010; Holmboe and Bourg, 2013; Zhang et al., 2014). In that case, water molecules do not have obviously preferred sites due to the 2-dimiension geometry of the pores. This comparison reveals the controls of crystal structure on the distribution of intracrystalline water.

This study further discloses that the zeolitic waters are indistinguishable and have much higher mobility than the bound water. However, the diffusion coefficients of zeolitic water are 1~2 orders of magnitude lower than that in montmorillonites, indicating much more limited mobility. Water in tunnels is more restricted than that in layered structures. That implies that materials with fibrous structures (1-dimension pores) could have more efficient fixation on water and other foreign small molecules adsorbed in tunnels such as CO_2, NH_3, SO_2, and so on in environmental applications.

It is well indicated that pore size or interlayer spacing could affect the mobility of interlayer water of montmorillonite (Holmboe and Bourg, 2013). Palygorskite, another widely utilized fibrous clay mineral, has smaller ribbon width than sepiolite. So, the zeolitic water in palygorskite may have lower mobility. Sepiolite is a pure trioctahedral mineral in nature, and it is found that some zeolitic water could be attracted by the hydroxyl of sepiolite trioctahedra. But, palygorskite always contains octahedral substitutions (Bergaya and Lagaly, 2013), therefore palygorskite with different octahedral substitutions may have various tunnel water distributions. Due to similar fibrous

296 structures, the other minerals in palygorskite-sepiolite group may also have their own
297 specific water distribution sites and fixation on foreign molecules and ions. This will be
298 addressed in a near future molecular simulation study.

ACKNOWLEDGMENT

We are grateful to the fruitful discussion with Dr. Randall T. Cygan. And we acknowledge National Science Foundation of China (Nos. 41425009 and 41222015) and the financial support from the State Key Laboratory for Mineral Deposits Research. We are grateful to the High Performance Computing Center of Nanjing University for using the IBM Blade cluster system.

References

Anderson, J.A., Daza, L., Fierro, J.L.G., Rodrigo, M.T. (1993) Influence of preparation method on the characteristics of nickle sepiolite catalysts. Journal of the Chemical Society-Faraday Transactions, 89, 3651-3657.

Anderson, R.L., Ratcliffe, I., Greenwell, H.C., Williams, P.A., Cliffe, S., Coveney, P.V. (2010) Clay swelling—a challenge in the oilfield. Earth-Science Reviews, 98, 201-216.

Benli, B., Du, H., Celik, M.S. (2012) The anisotropic characteristics of natural fibrous sepiolite as revealed by contact angle, surface free energy, AFM and molecular dynamics simulation. Colloids and Surfaces A-Physicochemical and Engineering Aspects, 408, 22-31.

Bergaya, F., Lagaly, G. (2013) Handbook of clay science. Elsevier, Developments of Clay Science, Volume 1, Amsterdam.

Brauner, K., Preisinger, A. (1956) Struktur und entstehung des sepioliths. Tschermaks Mineralogische und Petrographische Mitteilungen, 6, 120-140.

Brigatti, M.F., Medici, L., Poppi, L. (1996) Sepiolite and industrial waste-water purification: removal of Zn^{2+} and Pb^{2+} from aqueous solutions. Applied Clay Science, 11, 43-54.

Bukas, V.J., Tsampodimou, M., Gionis, V., Chryssikos, G.D. (2013) Synchronous ATR infrared and NIR-spectroscopy investigation of sepiolite upon drying. Vibrational Spectroscopy, 68, 51-60.

Caturla, F., Molina-Sabio, M., Rodriguez-Reinoso, F. (1999) Adsorption-desorption of water vapor by natural and heat-treated sepiolite in ambient air. Applied Clay Science, 15, 367-380.

Celis, R., Hermosin, M.C., Cornejo, J. (2000) Heavy metal adsorption by functionalized clays. Environmental Science & Technology, 34, 4593-4599.

Cygan, R.T., Liang, J.-J., Kalinichev, A.G. (2004) Molecular models of hydroxide, oxyhydroxide, and clay phases and the development of a general force field. The Journal of Physical Chemistry B, 108, 1255-1266.

Darder, M., Aranda, P., Ruiz-Hitzky, E. (2007) Bionanocomposites: A new concept of ecological, bioinspired, and functional hybrid materials. Advanced Materials, 19, 1309-1319.

Delgado, J.A., Uguina, M.A., Sotelo, J.L., Ruíz, B., Rosário, M. (2007) Carbon dioxide/methane separation by adsorption on sepiolite. Journal of Natural Gas Chemistry, 16, 235-243.

Dogan, M., Ozdemir, Y., Alkan, M. (2007) Adsorption kinetics and mechanism of cationic methyl violet and methylene blue dyes onto sepiolite. Dyes and Pigments, 75, 701-713.

Frost, R.L., Ding, Z. (2003) Controlled rate thermal analysis and differential scanning calorimetry of sepiolites and palygorskites. Thermochimica Acta, 397, 119-128.

Galan, E. (1996) Properties and applications of palygorskite-sepiolite clays. Clay Minerals, 31, 443-453.

Giustetto, R., Levy, D., Wahyudi, O., Ricchiardi, G., Vitillo, J.G. (2011a) Crystal structure refinement of a sepiolite/indigo Maya Blue pigment using molecular modelling and synchrotron diffraction. European Journal of Mineralogy, 23, 449-466.

Giustetto, R., Wahyudi, O., Corazzari, I., Turci, F. (2011b) Chemical stability and dehydration behavior of a sepiolite/indigo Maya Blue pigment. Applied Clay Science, 52, 41-50.

Gupta, V.K., Suhas (2009) Application of low-cost adsorbents for dye removal - A review. Journal of Environmental Management, 90, 2313-2342.

He, C.L., Makovicky, E., Osbaeck, B. (1996) Thermal treatment and pozzolanic activity of sepiolite.

Applied Clay Science, 10, 337-349.

Holmboe, M., Bourg, I.C. (2013) Molecular dynamics simulations of water and sodium diffusion in smectite interlayer nanopores as a function of pore size and temperature. The Journal of Physical Chemistry C, 118, 1001-1013.

Hubbard, B., Kuang, W., Moser, A., Facey, G.A., Detellier, C. (2003) Structural study of Maya Blue: textural, thermal and solid-state multinuclear magnetic resonance characterization of the palygorskite-indigo and sepiolite-indigo adducts. Clays and Clay Minerals, 51, 318-326.

Kara, M., Yuzer, H., Sabah, E., Celik, M.S. (2003) Adsorption of cobalt from aqueous solutions onto sepiolite. Water Research, 37, 224-232.

Martin, M.G. (2013) MCCCS Towhee: a tool for Monte Carlo molecular simulation. Molecular Simulation, 39, 1212-1222.

Ockwig, N.W. et al. (2009) Nanoconfined water in magnesium-rich 2:1 phyllosilicates. Journal of the American Chemical Society, 131, 8155-8162.

Ozcan, A., Ozcan, A.S. (2005) Adsorption of Acid Red 57 from aqueous solutions onto surfactant-modified sepiolite. Journal of Hazardous Materials, 125, 252-259.

Plimpton, S., Crozier, P., Thompson, A. (2007) LAMMPS-large-scale atomic/molecular massively parallel simulator. Sandia National Laboratories.

Post, J.E., Bish, D.L., Heaney, P.J. (2007) Synchrotron powder X-ray diffraction study of the structure and dehydration behavior of sepiolite. American Mineralogist, 92, 91-97.

Preisinger, A. (1959) X-ray study of the structure of sepiolite. Clays and Clay Minerals, 6, 61-67.

Rautureau, M., Mifsud, A. (1977) Electron-microscopy of different hydration states of sepiolite. Clay

Minerals, 12, 309-318.

Ruiz-Hitzky, E. (2001) Molecular access to intracrystalline tunnels of sepiolite. Journal of Materials Chemistry, 11, 86-91.

Rytwo, G., Tropp, D., Serban, C. (2002) Adsorption of diquat, paraquat and methyl green on sepiolite: experimental results and model calculations. Applied Clay Science, 20, 273-282.

Samper-Madrigal, M.D., Fenollar, O., Dominici, F., Balart, R., Kenny, J.M. (2015) The effect of sepiolite on the compatibilization of polyethylene-thermoplastic starch blends for environmentally friendly films. Journal of Materials Science, 50, 863-872.

Sanchez, C., Belleville, P., Popall, M., Nicole, L. (2011) Applications of advanced hybrid organic-inorganic nanomaterials: from laboratory to market. Chemical Society Reviews, 40, 696-753.

Shariatmadari, H., Mermut, A.R., Benke, M.B. (1999) Sorption of selected cationic and neutral organic molecules on palygorskite and sepiolite. Clays and Clay Minerals, 47, 44-53.

Sheikhhosseini, A., Shirvani, M., Shariatmadari, H., Zvomuya, F., Najafic, B. (2014) Kinetics and thermodynamics of nickel sorption to calcium-palygorskite and calcium-sepiolite: A batch study. Geoderma, 217, 111-117.

Shimizu, K.-i., Maruyama, R., Komai, S.-i., Kodama, T., Kitayama, Y. (2004) Pd–sepiolite catalyst for Suzuki coupling reaction in water: structural and catalytic investigations. Journal of Catalysis, 227, 202-209.

Tambach, T.J., Hensen, E.J.M., Smit, B. (2004) Molecular simulations of swelling clay minerals. Journal of Physical Chemistry B, 108, 7586-7596.

Tsampodimou, M., Bukas, V.-J., Stathopoulou, E.T., Gionis, V., Chryssikos, G.D. (2015) Near-infrared investigation of folding sepiolite. American Mineralogist, 100, 195-202.

Vico, L. (2003) Acid–base behaviour and Cu^{2+} and Zn^{2+} complexation properties of the sepiolite/water interface. Chemical geology, 198, 213-222.

Zhang, L.H., Lu, X.C., Liu, X.D., Zhou, J.H., Zhou, H.Q. (2014) Hydration and Mobility of Interlayer Ions of (Nax, Cay)-Montmorillonite. A Molecular Dynamics Study. The Journal of Physical Chemistry C, 118, 29811-29821.

Zheng, Y.G., Ye, H.F., Zhang, Z.Q., Zhang, H.W. (2012) Water diffusion inside carbon nanotubes: mutual effects of surface and confinement. Physical Chemistry Chemical Physics, 14, 964-971.

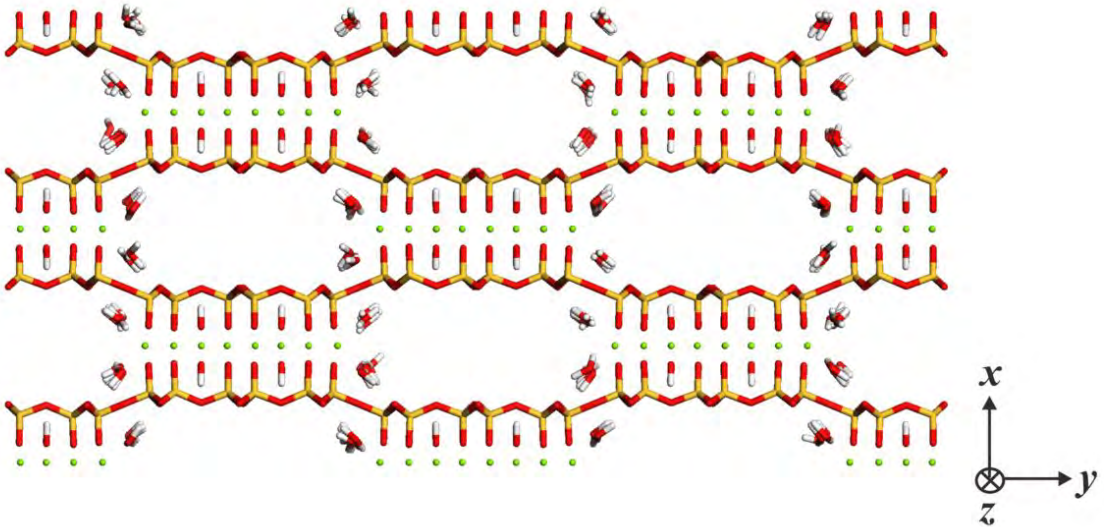
x
y
z

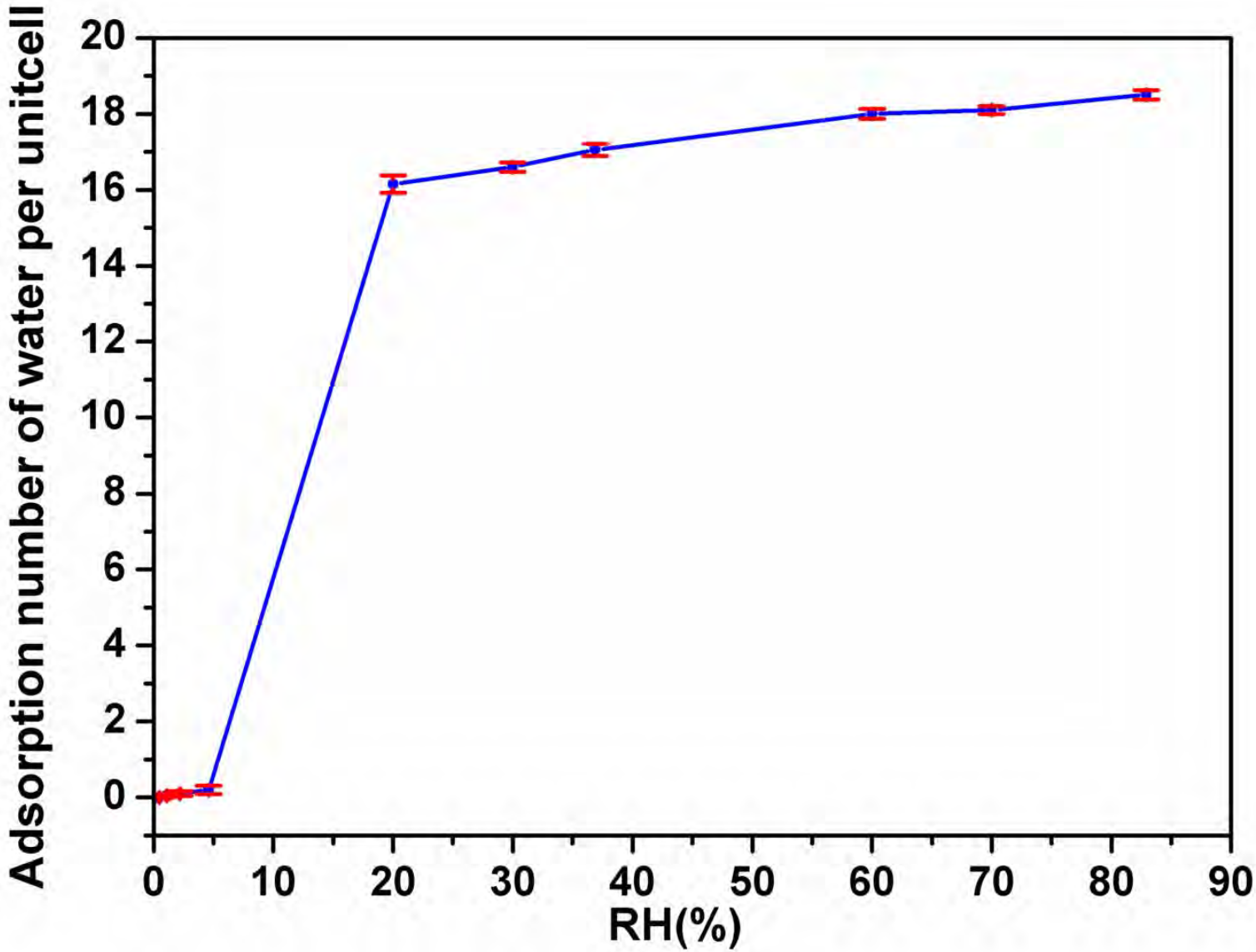
Adsorption number of water per unitcell
20
18
16
14
12
10
8
6
4
2
0
0
10
20
30
40
50
60
70
80
90
RH(%)

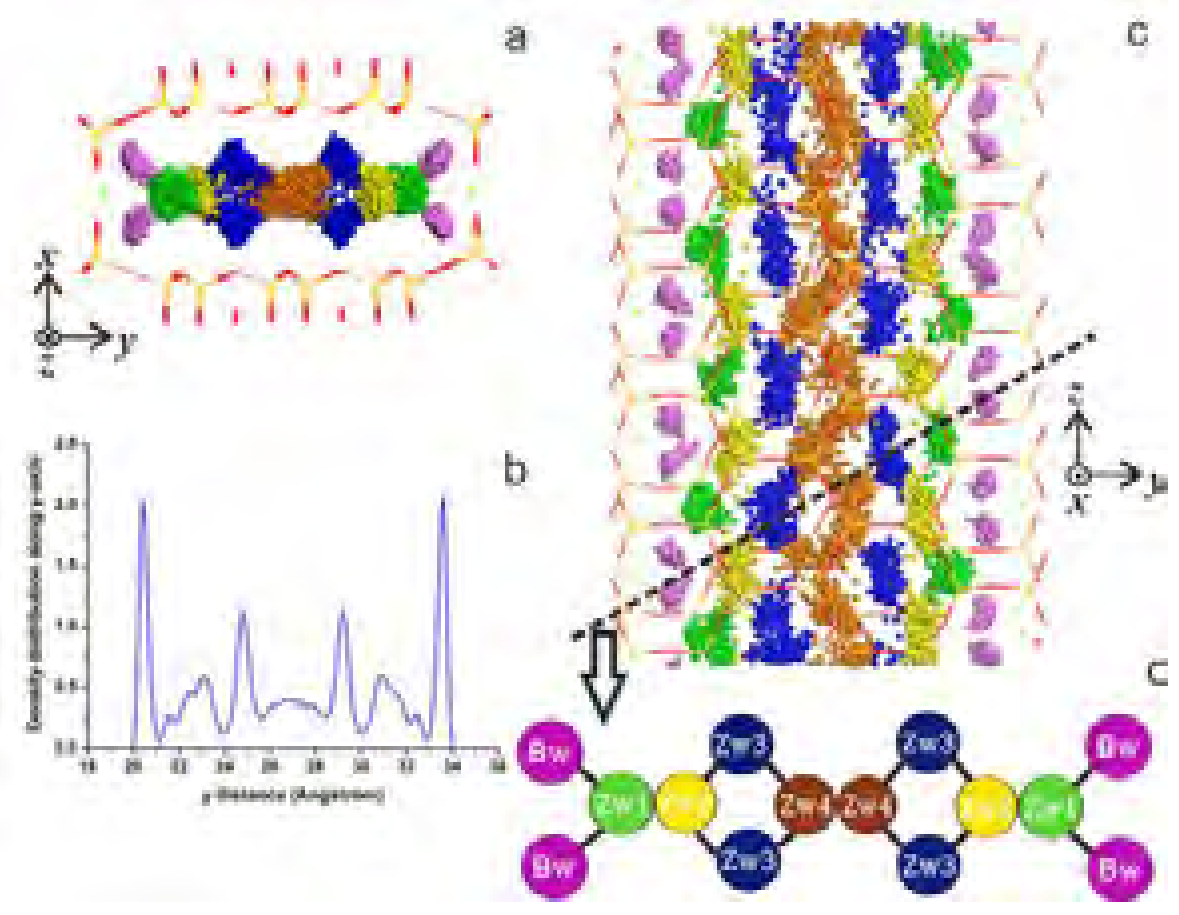
a
b
c
c
z
y
x
y
Bw
Zw1
Zw3
Zw4
Zw3
Zw4
Zw1
Bw
Bw
Zw3
Zw3
Bw

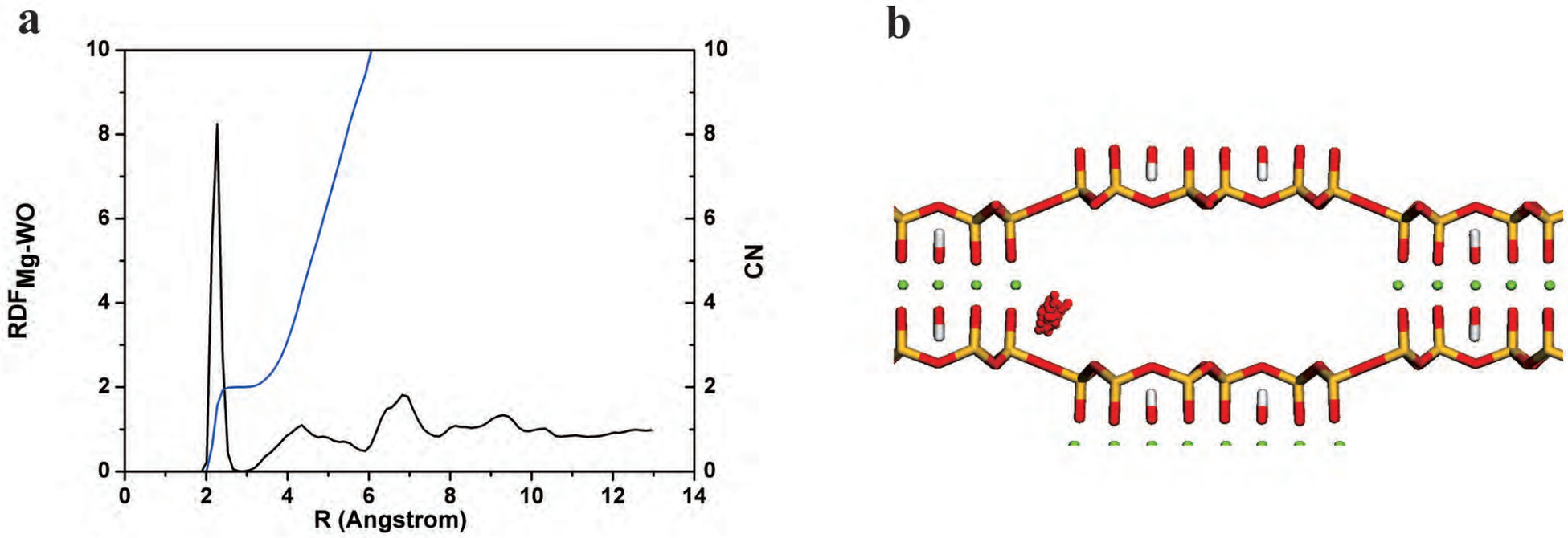
a
b
RDF Mg-WO
CN
R (Angstrom)
0
2
4
6
8
10
12
14

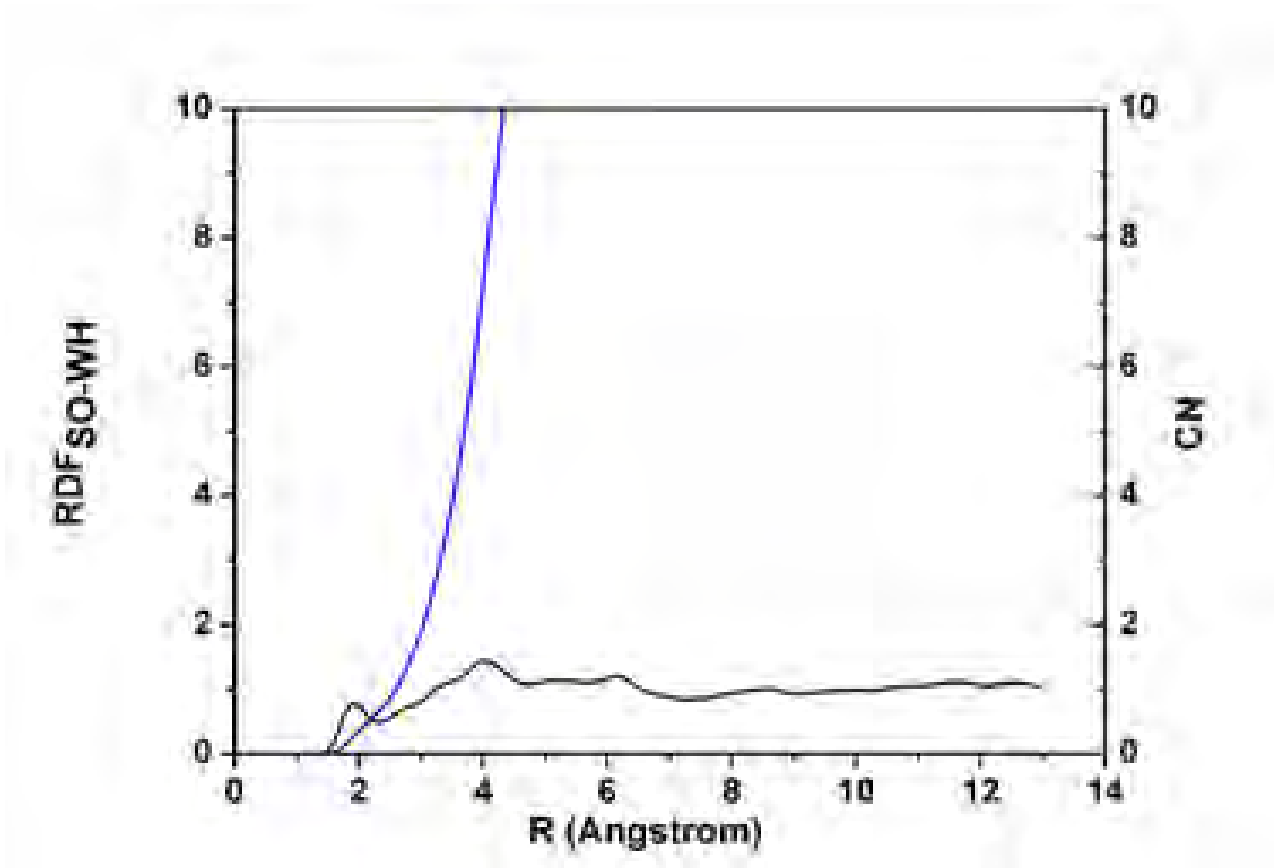
RDFSO-WH
CN
R (Angstrom)
0
2
4
6
8
10
12
14


(a) Zw1
(b) Zw2
(c) Zw3
(d) Zw4

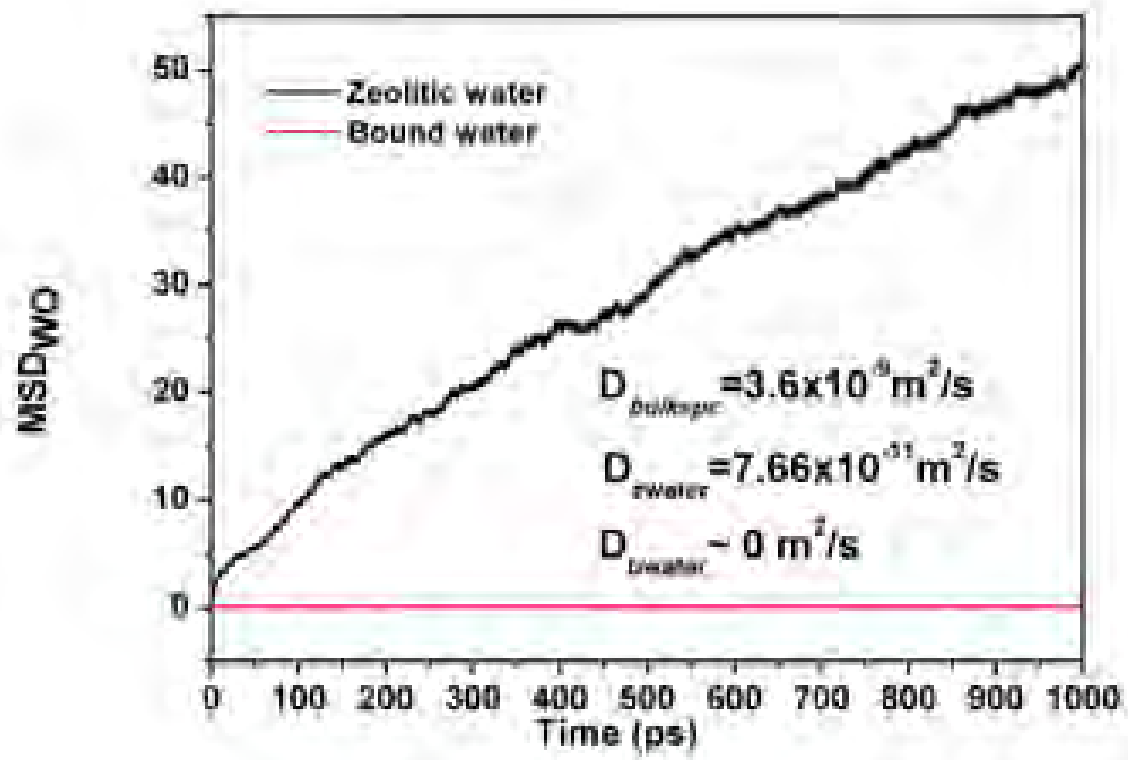
Zeolitic water
Bound water
$D_{bulkspc}$=3.6x10^{-9}m^2/s
D_{zwater}=7.66x10^{-11}m^2/s
D_{bwater}~ 0 m^2/s
MSD$_{WO}$
Time (ps)
0
10
20
30
40
50
0
100
200
300
400
500
600
700
800
900
1000